Understanding reaction mechanisms using dynamic electrochemical impedance spectroscopy: Methanol oxidation on Pt

Thomas Holm, Svein Sunde, Frode Seland, David A. Harrington

November 2019

Accepted version of Electrochim. Acta, 323 (2019) 134764. doi: 10.1016/j.electacta.2019.134764

Understanding reaction mechanisms using dynamic electrochemical impedance spectroscopy: Methanol oxidation on Pt

Thomas Holm[a,**], Svein Sunde[b], Frode Seland[b], David A. Harrington[a,*]

[a] *Department of Chemistry, University of Victoria, Victoria, British Columbia, V8W 2Y2, Canada.*
[b] *Department of Materials Science and Engineering, Norwegian University of Science and Technology (NTNU), NO-7491 Trondheim, Norway.*

Abstract

Data from a combined cyclic voltammetry and dynamic electrochemical impedance spectroscopy (dEIS) study of the methanol oxidation reaction (MOR) at high temperatures was revisited using a new method for mechanistic modeling. Through iterative optimization of kinetic parameters, a total of five reaction mechanisms of the indirect pathway of the MOR were modeled. The calculated dEIS spectra from the kinetic parameters were used to verify the reaction mechanisms and best fits were found where i) water adsorption is reversible and hinders the MOR at lower potentials (< 0.50 V vs RHE), and ii) the surface reaction between adsorbed CO and OH is chemical.

Keywords:
Dynamic Electrochemical Impedance Spectroscopy, Methanol Oxidation, Temperature, Reaction Mechanism

1. Introduction

Electrochemical impedance spectroscopy (EIS) is a powerful tool for understanding reaction mechanisms. In particular, EIS measured over a wide frequency range has been used to identify mass-transport limitations, adsorption processes, and individual elementary reaction steps from the frequency dependence. While EIS spectra are uniquely dense in information among electrochemical techniques, interpretation of the data is complicated and an already good understanding of the system is necessary for reliable interpretation. Through a good understanding, a reaction mechanism can be stated and the kinetic parameters can be fitted to experimental data. This approach has been used to understand electrochemical reactions, particularly in the field of corrosion [1–4]. While these notable exceptions occur, such an interpretation sets a high demand of the experimenter, and the interpretation of EIS data is often limited to pattern recognition or the fitting of arbitrary electrical equivalent circuits [5].

In the dynamic EIS (dEIS) method, a multi-sine ac perturbation is imposed on the quasi steady-state electrochemical technique, cyclic voltammetry. The advantage of dEIS for mechanistic interpretation is that two electrochemical techniques are measured simultaneously at the same surface conditions. This aspect allows for a two-step interpretation where kinetic parameters for a given reaction mechanism can be fitted to the cyclic voltammetry data and subsequently be used to calculate the dEIS spectra at given potentials. The relationship between spectral features and reaction steps is indirect. However, distinct shapes of dEIS spectra for voltammograms that are similar is effective in distinguishing reaction mechanisms. This approach, supported by literature date from spectroscopic techniques such as IR spectroscopy and differential electrochemical mass spectroscopy (DEMS), provides a pathway to understand reaction mechanisms in greater detail.

The definition of dynamic impedance in terms of Volterra series by Battistel and La Mantia [6] gives a formal justification of the earlier heuristic treatments of dynamic impedance by us and others. These earlier treatments made the reasonable assumption that an impedance could be defined so long as the potential, coverages and other physical parameters did not change too much during an ac cycle, and various estimates were presented as to how low in frequency it was possible to go for a particular CV sweep rate [7–12]. Although in principle the lowest frequency depends on the system time constants [12], in practice we have found that 1 Hz at 5 mV s^{-1} is measurable and gives results conforming with the Kramers-Kronig (KK) transform. In the present case, the dEIS spectra were fitted successfully to KK compliant equivalent circuits [13]. Another test for valid data was that the polarization resistances from the fitted low-frequency limits agreed with the inverse slopes of the slow-sweep current-potential curves, at least for the 100°C data analysed here [13].

A recent dEIS study of methanol oxidation on Pt at

*Corresponding author. Tel.: +1-250-721-7166
**Current address: Clean Energy Research Centre (CERC), University of British Columbia, Vancouver, British Columbia, V6T 1Z4, Canada.
Email addresses: thomas.holm@ubc.ca (Thomas Holm), svein.sunde@ntnu.no (Svein Sunde), frode.seland@ntnu.no (Frode Seland), dharr@uvic.ca (David A. Harrington)

high temperatures [13] focused on how the mechanism changes with temperature. A qualitative discussion of the mechanism was given, but there was no analysis at the level of rate constants. Here a detailed kinetic analysis at one temperature is used to extract rate constants, and directly compare potential reaction mechanisms. The computational detail of the fitting method used here were recently given a preliminary report [14]. The reaction mechanisms here are all variations of methanol oxidation proceeding through the indirect pathway, i.e., through adsorbed CO. In total, five different reaction mechanisms are modeled and used to calculate dEIS spectra. The ability to directly compare competing models against each other and against data from two simultaneously-acquired experimental methods gives confidence about which aspects of these mechanisms are reliable. It is shown that i) water adsorption is a reversible process, and ii) the surface reaction between adsorbed OH and CO is a chemical reaction, i.e., a Kauranen step [15]. The interpretation method used here has wide application, in particular where a) the EIS spectra have several distinct features and b) a rough understanding of the reaction mechanism has been established previously.

2. Experimental

2.1. Conventional electrochemistry

A commercially available autoclave (BüchiGlasUster AG) was custom fitted for electrochemical experiments as described in previous work [16, 17]. The experimental procedure is explained in the previous work on this system [13]. Temperatures were calibrated and have an estimated error of ±3 K. The solutions used were all produced from ultrapure water (Millipore Milli-Q 18 MΩ cm), sulfuric acid (SeaStar Baseline) and methanol (Alfa Aesar >99.9 %). The experiments were conducted in 0.5 M sulfuric acid with and without 1 M methanol. All experiments used 200 mL total electrolyte volume. The working electrode and counter electrodes were platinum wires sealed in glass (geometric area about 0.01 cm^2 for the working electrode and 0.08 cm^2 for the counter electrode), and the reference electrode was a reversible hydrogen electrode (RHE) in the same electrolyte. All potentials are reported vs this reference electrode.

A Gamry Ref 600 potentiostat was used for all experiments. Before methanol was added to the solution, the electrochemically active surface area of the working electrode was calculated from the integration of hydrogen adsorption peaks during cyclic voltammograms at 100 mV s^{-1} at room temperature between 70 and 300 mV. The active area was determined to be 0.015 cm^2 assuming 220 μC per cm^2 of active area. The area was assumed to be independent of temperature.

Dynamic EIS was run using in-house software and hardware as described in previous publications [11, 12]. Impedance was measured with a minimum frequency of 1 Hz, maximum frequency of 13 kHz, and a maximum total amplitude of 30 mV. The selected frequencies were chosen after the system described by Popkirov [18], and the signal amplitude was halved for every decade increase in frequency. DEIS was run with CVs at 5 mV s^{-1}. The post-processing allows for impedance spectra to be calculated at any potential during the continuous sweep, using data over 1 s centered at that potential. Data recorded at 100°C are analyzed in this work.

2.2. Modeling of the MOR

The modeling of the MOR was done in Maple (v. 2015.2, Maplesoft), with the detailed procedure described in a recent publication [14]. Briefly, the stated reaction mechanisms were set up as a system of ordinary differential equations involving adsorbed species at the electrode and solved for the conditions of the cyclic voltammetry experiment. In order to obtain convergence, the parameters were first adjusted manually to ensure stability ($j \neq 0$ in the whole fitted interval) and a rough resemblance to the experimental voltammogram. Subsequently, the least-squares error was calculated based on the experimental data and each parameter was optimized independently in sequence by using the built-in non-linear program solver (NLPsolve) with either the nonlinearsimplex or the branch-and-bound option. This iterative process was repeated until a full iteration gave less than 0.01 % improvement of the error function from the previous iteration. Satisfactory convergence was obtained in fewer than 30 iterations. From the optimized models, the EIS spectra were calculated at selected potentials according to established methodology [19, 20].

Standard errors were estimated from numerical derivatives of $\log_{10} j$ with respect to the parameters, which were the logarithms (base 10) of the rate constants. Specifically, the partial derivatives were approximated by the 5 point stencil formula (Eq. 3.4.9, Ref. [21] with $t = 0$) using step length $h = 10^{-4}$. These were then converted to standard errors in $\log_{10} k_i$ using the usual first-order analysis [22].

3. Results and discussion

3.1. The methanol oxidation reaction mechanism

The methanol oxidation reaction (MOR) on platinum in acidic solution proceeds through a dual pathway mechanism. The direct pathway proceeds through short-lived or no adsorbates to produce formaldehyde, formic acid, or CO_2. The indirect pathway proceeds through strongly adsorbed CO to CO_2. At room temperature, MOR produces a relatively low fraction of CO_2, indicating that the direct mechanism is the main reaction pathway. At higher temperatures, in particular at 100°C, the reaction produces almost exclusively CO_2 [23]. The low fraction of partial oxidation products, formaldehyde and formic acid, indicates that the indirect pathway plays a major role and we assume that it explains the measured current.

Before stating the reaction mechanism, the key literature observations behind the suggested mechanism are the following:

(1) Methanol oxidation at potentials below 0.5 V leads to adsorbed CO at the surface. This is assumed to be the dominant adsorbed reaction intermediate [24, 25].

(2) Multiple Pt sites are necessary for methanol adsorption and dehydrogenation to CO [26–28].

(3) CO coverage is at a maximum at the onset of CO oxidation and decreases as the potential increases [29–31].

(4) Dissociative water adsorption is reversible and not considered a possible rate-determining step (except that it hinders CO oxidation at potentials below where water adsorption can occur) [32, 33].

(5) Formation of platinum oxide at high potentials reduces the methanol oxidation current drastically and is the major reason for the current drop past 0.8 V.

Based on these literature findings and our previous experimental results [13], a reaction pathway for the indirect mechanism was suggested and is given below in Eqs. (1)-(6).

$$3\mathrm{Pt} + \mathrm{CH_3OH} \xrightarrow{k_{\mathrm{CH_2OH}}} \mathrm{Pt_3CH_2OH} + \mathrm{H^+} + \mathrm{e^-} \quad (1)$$

$$\mathrm{Pt_3CH_2OH} \xrightarrow{k_{\mathrm{CO}}} \mathrm{PtCO} + 2\mathrm{Pt} + 3\mathrm{H^+} + 3\mathrm{e^-} \quad (2)$$

$$\mathrm{Pt} + \mathrm{H_2O} \underset{k_{-\mathrm{OH}}}{\overset{k_{\mathrm{OH}}}{\rightleftharpoons}} \mathrm{PtOH} + \mathrm{H^+} + \mathrm{e^-} \quad (3)$$

$$\mathrm{PtCO} + \mathrm{PtOH} \xrightarrow{k_{\mathrm{COOH}}} \mathrm{PtCOOH} + \mathrm{Pt} \quad (4)$$

$$\mathrm{PtCOOH} \xrightarrow{k_{\mathrm{CO_2}}} \mathrm{CO_2} + \mathrm{Pt} + \mathrm{H^+} + \mathrm{e^-} \quad (5)$$

$$\mathrm{PtOH} \underset{k_{-\mathrm{PtO}}}{\overset{k_{\mathrm{PtO}}}{\rightleftharpoons}} \mathrm{PtO} + \mathrm{H^+} + \mathrm{e^-} \quad (6)$$

Here, the prefix Pt or Pt_3 symbolizes an adsorbed molecule, $\rightarrow$ means an irreversible reaction, $\rightleftharpoons$ means an equilibrium reaction, and Pt means an available Pt site. The model stated in Eqs. (1)-(6) is called 3Ceq in this work and considered the baseline model. For the calculations, the symmetry coefficient was fixed at 0.5 for all electrochemical steps except for Eq. (1) where 0.75 was used according to first principles calculations in the literature [34, 35]. Although Eq. (2) is given as a single step transferring three electrons, it is almost certainly a composite step. Since the adsorbed intermediates between Pt_3CH_2OH and CO have not been observed experimentally, the first electron transfer of the three is assumed to be the slow substep, with subsequent substeps much faster. Therefore the kinetics are equivalent to a single step with symmetry coefficient 0.5.

Within the mechanistic framework of Eqs. (1)-(6), we focus on three testable aspects. Although these have been discussed already in the literature, the present method enables direct comparison of competing mechanisms.

The first aspect is the role of vacant sites required for the initial dissociative adsorption of methanol, Eq. (7). Here, x is a value between 2 and 4; most commonly 3 has been used in the literature. We seek to better determine the value of x.

$$x\mathrm{Pt} + \mathrm{CH_3OH} \xrightarrow{k_{\mathrm{CH_2OH}}} \mathrm{Pt}_x\mathrm{CH_2OH} + \mathrm{H^+} + \mathrm{e^-} \quad (7)$$

The second aspect is to determine whether or not the water adsorption step can be considered at equilibrium. If at equilibrium, the coverage of PtOH is strictly a function of the number of available sites and the potential as in Eq. (8). The equilibrium assumption is tested simultaneously for the PtO formation reaction, Eq. (6), and leads to Eq. (9).

$$\frac{\theta_{\mathrm{OH}}}{\theta_{\mathrm{Pt}}} = K_{\mathrm{OH}} \exp\left(\frac{FE}{RT}\right) \quad (8)$$

$$\frac{\theta_{\mathrm{PtO}}}{\theta_{\mathrm{OH}}} = K_{\mathrm{PtO}} \exp\left(\frac{FE}{RT}\right) \quad (9)$$

Here, θ_i is the coverage of species i, K_{OH} and K_{PtO} are the equilibrium constants at $E = 0$, F is the Faraday constant, E is the potential relative to 0 V vs RHE, R is the gas constant, and T is the temperature. Note also that in the equilibrium constants, K_{OH} and K_{PtO}, the dependency on proton concentration is already incorporated and assumed constant in this work.

The third aspect is to test whether the surface reaction between CO and OH is chemical or electrochemical in nature. Kauranen et al [15] have suggested that it is chemical and this has yielded good fit with experimental data [2] for the MOR. The chemical surface reaction is given as the steps in Eqs. (4)-(5). Alternatively, if it were a single electrochemical step, it would be given directly as in Eq. (10).

$$\mathrm{PtCO} + \mathrm{PtOH} \xrightarrow{k_{\mathrm{CO2}}} 2\mathrm{Pt} + \mathrm{CO_2} + \mathrm{H^+} + \mathrm{e^-} \quad (10)$$

To test the three aspects mentioned above, five reaction mechanisms were considered and these are summarized in Table 1. The models are named as 3|C|eq by first the number of sites for aspect 1, then denoting the type of surface reaction as (C)hemical or (E)lectrochemical for aspect 3, and last by the type of reaction for water adsorption in aspect 2, either (eq)uilibrium or (No) (Eq)uilibrium. Models 2Ceq, 3Ceq, and 4Ceq compare different number of Pt sites for methanol adsorption, model 3CNoEq compared to 3Ceq investigates the nature of the water adsorption reaction, and model 3Eeq compared to 3Ceq investigates the nature of the surface reaction between CO and OH.

3.2. Modeling and optimization of the methanol oxidation reaction

All the five models that were suggested converged successfully as shown in Fig. 1. Here, the residual sum of squares (RSS) function as given in Eq. (11) gives the total non-normalized error, and a total of 81 experimental

Table 1: The models used for Maple modeling of the methanol oxidation reaction

Model	2Ceq	3Ceq	4Ceq	3CNoEq	3Eeq
x, number of sites for methanol adsorption	**2**	3	**4**	3	3
Equilibrium OH / PtO	Y	Y	Y	**N**	Y
Chemical surface reaction	Y	Y	Y	Y	**N**

data points between 0.55 V and 0.95 V were used for the minimization of RSS.

$$RSS = \sum_{i=1}^{81} (\log_{10}(j_{i,\mathrm{exp}}) - \log_{10}(j_{i,\mathrm{mod}}))^2 \qquad (11)$$

Here, $j_{i,\mathrm{exp}}$ is the experimental data point, and $j_{i,\mathrm{mod}}$ is the model data point. The fitted parameters, both in linear and logarithmic form, are given in Table 2.

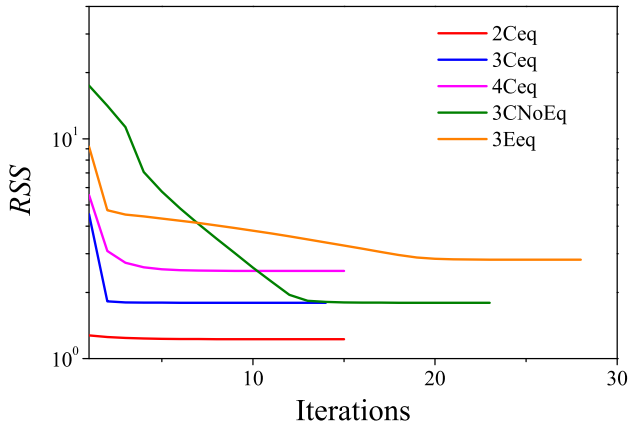

Figure 1: The error function, RSS, as a function of the number of iterations in the optimization procedure.

From the procedure used to estimate the standard error of the parameters, it is evident that some parameters cannot be determined with any certainty. This is expected for parameters whose values are not important in determining the rate, and can be used as an indication of which parameters are rate-determining or partly rate-determining in the potential window modeled. For example, the rate constant of a fast step following a slow step will have a rate constant whose value is much larger than for the slow step, but not well determined, as is the case here for k_{CO} compared to k_{CH2OH}. Likewise, a reaction in near equilibrium will have forward and reverse rate constants that are large enough to ensure equilibrium, but only their ratio will be well determined, as is the case here with k_{OH} and $k_{-\mathrm{OH}}$.

For all of the models, the rate constant for methanol adsorption, k_{CH2OH}, and the rate constant for the surface reaction, either k_{CO2} (for 3Eeq) or k_{COOH} (for all other models), could be determined. In addition, the water adsorption reaction could be estimated for the reaction mechanism where this reaction is not reversible, 3CNoEq. This can be expected as for all other mechanisms, the surface coverage of water is found according to Eq. (8), and thus only the ratio $k_{\mathrm{OH}}/k_{-\mathrm{OH}}$ is significant. At the bottom of Table 2, the calculated ratio is given. All the models are in a similar range, indicating that this equilibrium constant can be determined with some accuracy, and likely has a significant influence on the overall current. Thus, from the error estimates, the possible rate-determining reactions are methanol adsorption, Eq. (1), the water adsorption reaction, Eq. (3), and the surface reaction, Eq. (10) for the 3Eeq mechanism, and Eq. (4) for all other models.

3.3. Cyclic voltammetry

Simulated voltammograms based on the rate constants emerging from the fits are shown in Fig. 2. Here, the red box indicates the potential zone where the models were fitted. The more representative presentation is with a logarithmic scale on the vertical axis, i.e., Fig. 2b. Generally, all the models closely approximate the experimental curve including the shoulder peak. The fit quality, quantified by the RSS function, is given in Fig. 1, where 2Ceq gives the best fit, 3Ceq and 3CNoeq both have similar fits and are the second best overall, and the 4Ceq and 3Eeq models have the worst fit. This shows that the optimization procedure works well and can successfully converge to a realistic result.

The observation that all the models actually closely approximate the experimental data indicates that either i) they are all decent representations of the overall reaction, or ii) that the experimental method, cyclic voltammetry, does not have enough features to be able to distinguish between these models. The last point is a general problem when attempting to model experimental results, especially with steady-state techniques. In the case of methanol oxidation, the reaction mechanism of the indirect mechanism has been known to a greater or lesser detail since the nature of the strongly adsorbed adsorbate was determined in the late 1980's [24]. Thus, all the models represent the reaction mechanism to some degree, but cyclic voltammetry is not able to distinguish between them.

3.4. Adsorbate coverages

The surface coverages of the adsorbates are a direct output of the modeling and are shown for the five models in Fig. 3a-f. IR spectroscopy has been shown to qualitatively give the surface coverage as a function of potential and temperature, as exemplified by numerous works [29–31]. However, limited information is available at high

Table 2: Optimized rate parameter values for the five different reaction models. The quoted errors are the estimated standard errors (1σ) for the logarithm of the rate constants, which were the parameters optimized in the fit. Errors in $\log_{10}(k_i)$ are omitted where the estimated standard error was larger than 1, i.e., the rate constants are uncertain by more than a factor of 10. In those cases, the rate constants are enclosed in parentheses. All the rate constants have units of mol m^{-2} s^{-1}.

Parameter	2Ceq	3Ceq	4Ceq	3CNoEq	3Eeq
k_{CH_2OH}	4.3×10^{-6}	4.4×10^{-6}	4.4×10^{-6}	3.7×10^{-6}	3.8×10^{-6}
$\log_{10}(k_{CH_2OH})$	-5.36 ± 0.01	-5.35 ± 0.01	-5.35 ± 0.02	-5.43 ± 0.01	-5.42 ± 0.01
k_{CO}	(10^{6})	(10^{9})	(10^{10})	(10^{1})	(10^{2})
$\log_{10}(k_{CO})$	6	9	10	1	2
k_{OH}	(10^{-5})	(10^{-5})	(10^{-5})	2.0×10^{-4}	(10^{-12})
$\log_{10}(k_{OH})$	-5	-5	-5	-3.71 ± 0.06	-12
k_{-OH}	(10^{8})	(10^{7})	(10^{8})	8.6×10^{8}	(10^{1})
$\log_{10}(k_{-OH})$	8	7	8	8.93 ± 0.08	1
k_{COOH}	9.6×10^{0}	1.6×10^{1}	2.7×10^{1}	1.4×10^{1}	n/a
$\log_{10}(k_{COOH})$	0.98 ± 0.02	1.22 ± 0.04	1.43 ± 0.05	1.13 ± 0.03	n/a
k_{CO_2}	(10^{6})	(10^{7})	(10^{7})	(10^{0})	2.3×10^{-3}
$\log_{10}(k_{CO_2})$	6	7	7	0	-2.64 ± 0.07
k_{PtO}	(10^{-10})	(10^{-12})	(10^{-4})	(10^{-17})	(10^{-26})
$\log_{10}(k_{PtO})$	-10	-12	-4	-17	-26
k_{-PtO}	(10^{38})	(10^{30})	(10^{24})	(10^{-15})	(10^{5})
$\log_{10}(k_{-PtO})$	38	30	24	-15	5
k_{OH}/k_{-OH}	4.0×10^{-13}	2.3×10^{-13}	1.6×10^{-13}	2.3×10^{-13}	2.0×10^{-13}
$\log_{10}(k_{OH}/k_{-OH})$	-12.4	-12.6	-12.8	-12.6	-12.7

temperatures. Thus, for the discussion of how the calculated surface coverages represent the real case, we assume that the general trend is similar at all temperatures as is the case for CO coverage during formic acid oxidation on Pt [36]. All of the models have similar trends in the CO coverage, going from a high CO coverage at low potentials to a low coverage at high potentials.

The maximum coverage of CO is also an interesting aspect. It is commonly assumed that the surface coverage of CO is limited to a maximum of about 0.7 when produced from methanol [26, 37–39] and that several sites are necessary for the reaction of methanol to CO [27, 28]. All of the models used here give a maximum coverage of about 0.90. While the value is higher than expected, the trend is realistic, and the addition of adsorbate interaction (repulsion) in the models would likely reduce the maximum coverage significantly. Other adsorption isotherms than the Langmuir isotherm were not included in this work to keep the number of parameters to be optimized at a minimum.

The OH coverage is difficult to determine experimentally, and is assumed to be closely related to the presence of PtO at higher potentials. Within the potential window, all models give no significant PtO coverage, and full OH coverage is observed at higher potentials. This effectively blocks the surface. Technically, the models allow for the OH formed to i) react with CO and form COOH (and then CO_2), or ii) react further to PtO. Case ii) is not favored because it is not necessary to fit the data, as OH can block the surface as well as PtO, resulting in a wide span of rates for PtO formation in the optimized models, see Table 2. The real case is more complex because the nature of the oxygen donor (OH in our case) and the initial stages of oxide formation are not well understood. As all the OH coverages are similar in the models, the cyclic voltammetry and surface coverage results indicate that the 2Ceq is the most realistic model. However, all models provided physically reasonable results and dEIS was further used to distinguish them.

3.5. Dynamic electrochemical impedance spectroscopy

Based on the fitted parameters, the impedance spectra at any potential can be calculated based on the general approach for a multistep reaction with adsorbed species [20, 40]. The result of this is presented in Fig. 4a-o as Nyquist, magnitude and phase angle plots for potentials between 0.50 V and 0.70 V. Similar to the work by Sundmacher and coworkers [2, 41], it is clear that models that look similar when modeling cyclic voltammetry or steady-state methods can have very different features when modeling impedance. The verification of the models is largely limited to pattern recognition, but some clear trends are visible: i) the modeled data fit the experimental data well at low overpotentials (< 0.60 V), but not as well at high overpotentials, ii) all the models give qualitatively similar

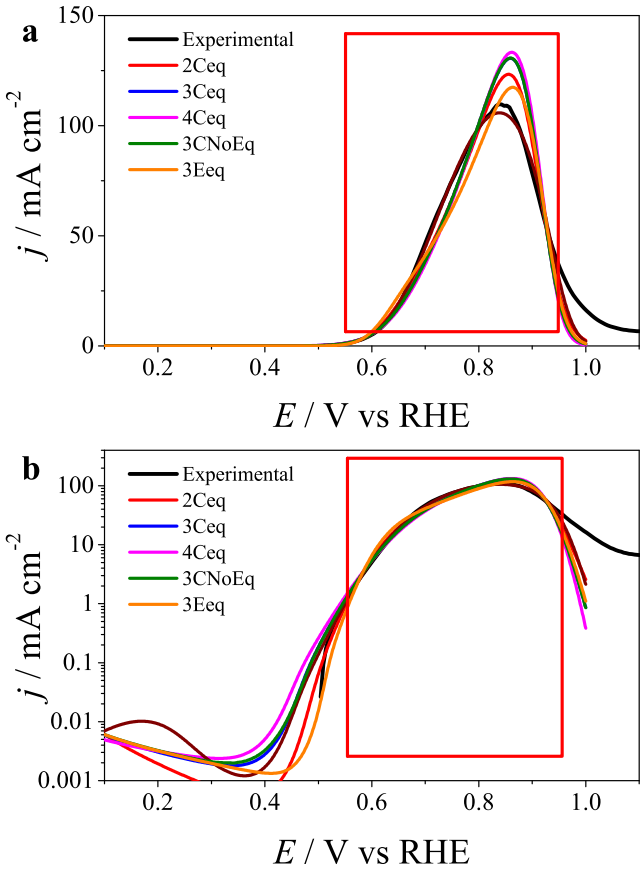

Figure 2: The results of Maple modeling of the reaction mechanisms showing the experimental cyclic voltammogram at 5 mV s^{-1} and at 100°C (black) along with the cyclic voltammograms modeled for model 2Ceq (red), 3Ceq (blue), 4Ceq (purple), 3CNoEq (green), and 3Eeq (orange). The potential zone used for the model fitting procedure is marked by the red box.

features, a capacitive loop at high frequencies and an inductive loop at low frequencies. In the case of 0.5 V, the data fit to a capacitive circuit and addition of an inductive loop was not statistically justified. As this potential is outside the fitting window, an extrapolation is involved and the modeling is less certain.

Considering that the cyclic voltammetry was modeled and dEIS spectra were calculated, the discrepancy observed between the model data and the experimental spectra is modest. Some discrepancy may be from the underlying assumption of only the indirect pathway, which can be challenged at potentials above 0.57 V where Chojak-Halseid and co-workers [23] observed a change in the CO_2 yield at 100°C from about 100% to about 93%. This means that the direct path has an influence at these potentials that is not accounted for in our work.

The second point is related to the similarity between the models. The inductive loop has been shown to be related to the change in CO coverage when the production and removal of CO have a comparable rate [13]. As all the models have a CO adsorbate incorporated and have similar trends in coverage as a function of potential, Fig. 3, a qualitatively similar feature is expected for all the models.

When comparing the key aspects of the models, the first question, the number of Pt sites necessary for methanol adsorption, the approach used here is inconclusive. From the EIS spectra, the 3Ceq and 4Ceq spectra give similar results, whereas the 2Ceq is similar at high potentials, and has a larger capacitive loop at lower potentials. A tentative conclusion is that the 3Ceq and 4Ceq models are the better representations of the experimental data. In our further comparisons, we assume that the results from single-crystal experiments and modeling [27, 28] hold and that 3 Pt sites are necessary for methanol dehydrogenation and adsorption. Of course, on a polycrystalline Pt surface, many different types of surface sites are present that might skew this picture.

The second aspect, whether or not water adsorption is reversible, can be decided by our work. The 3CNoEq model, which does not include the reversibility clearly has a third time-constant at lower frequencies, especially visible in Fig. 4a, d, and g. Notably, a slow irreversible adsorption of water leading to surface deactivation may explain the experimental difficulty with EIS in this potential range, as would be consistent with model 3CNoEq. However, this feature is at frequencies that are not accessible with the dEIS method and likely very hard to measure experimentally with a potentiostatic EIS measurement.

Notably, the 3Ceq model and the 3CNoEq model are almost identical, and looking closely at the parameters listed in Table 2, the ratio giving the equilibrium constant for water adsorption, $K_{OH} = k_{OH}/k_{-OH}$, is similar for the 3Ceq and 3CNoEq models. This is actually a general feature for all the models, and means that convergence is only reached for our models if water adsorption is at or near equilibrium. From this, the water adsorption parameters,

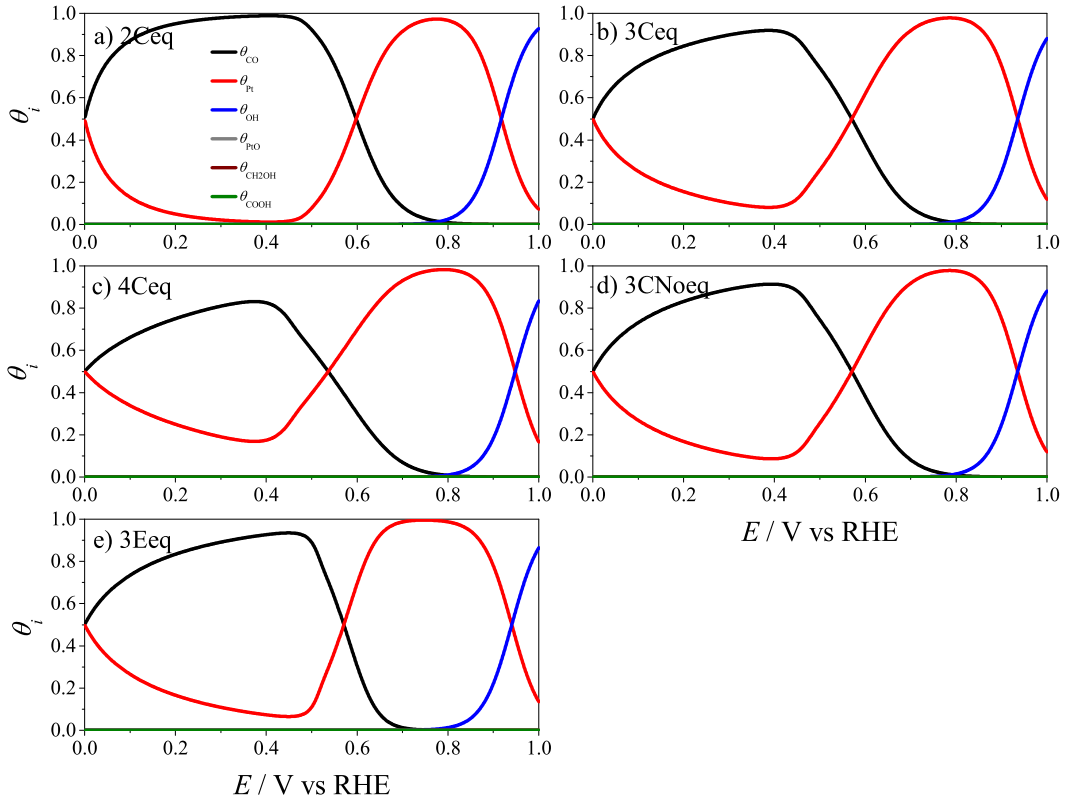

Figure 3: The surface coverage as a function of potential for the models a) 2Ceq, b) 3Ceq, c) 4Ceq, d) 3CNoEq, and e) 3Eeq.

k_{OH}/k_{-OH}, can be determined with high accuracy. This indicates that this step influences the starting point of the high rate methanol oxidation. The value of K_{OH} can be used to find the reversible potential for water adsorption. This can be done by finding the potential at the point where the CO and Pt coverages are equal, i.e., based on Eq. (8) to be where $1 = K_{OH}\exp(FE/RT)$. From this and the fitted parameters in Table 2, the equilbrium potential for water adsorption, E^{rev}_{OH}, can be determined to be between 0.92 and 0.95 V vs RHE.

The third aspect, the chemical or electrochemical nature of the surface reaction between adsorbed CO and OH, can be assessed by comparing the 3Ceq and the 3Eeq models. Here, the 3Eeq model has the worst RSS value in Fig. 1. However, when comparing the modeled dEIS results in Fig. 4, it has a poor fit at low potentials, while at higher potentials, above 0.60 V, it has a comparable fit with the other models. With the underlying assumptions in our models (fixed symmetry factors, no adsorbate interaction etc), the chemical surface reaction, model 3Ceq, gives a better fit than an electrochemical one, model 3Eeq, as has already been shown for this system in the literature [2, 15]. The tentative conclusion from the modeled dEIS data is that the 3Ceq and the 3CNoEq models are the more realistic models.

3.6. Revisiting the reaction mechanisms more closely

With the similarities being identified between the 3Ceq and 3CNoEq models, we can look at the 3Ceq model by calculating the rate of CO, r_{CO}, from the difference of the rate of the methanol adsorption step, Eq. (1), and the CO oxidation step, Eq. (4). This comparison is shown in Fig. 5 where in a) the experimental current and the resulting current from the 3Ceq model are plotted with the CO coverage, θ_{CO}, and in b) the difference between the CO production and removal step, $r_{CO} = v_1 - v_{COOH}$, is plotted with the CO coverage.

From Fig. 5b, one can see that the OH adsorption is activated slowly leading to CO removal and the CO rate, r_{CO}, is below zero from 0.37 V. At this potential, the overall rates are low and a small decrease in CO coverage is the result. Both of the reactions are activated by an increasing potential, and the CO oxidation rate is activated faster than the CO production rate at potentials above 0.4 V resulting in a more negative r_{CO}. At 0.46 V, there is a local minimum in CO rate. Prior to this, between 0.40 and 0.46 V, the overall rate is dominated by the rate of water activation, and the CO coverage is high. Beyond the local minimum, the CO coverage has dropped significantly enough so that both the rate of CO production and CO removal have a significant influence on the overall current. From 0.55 V to 0.90 V, the window modeled here, the dominant shape of the dEIS spectra is a capacitive loop at

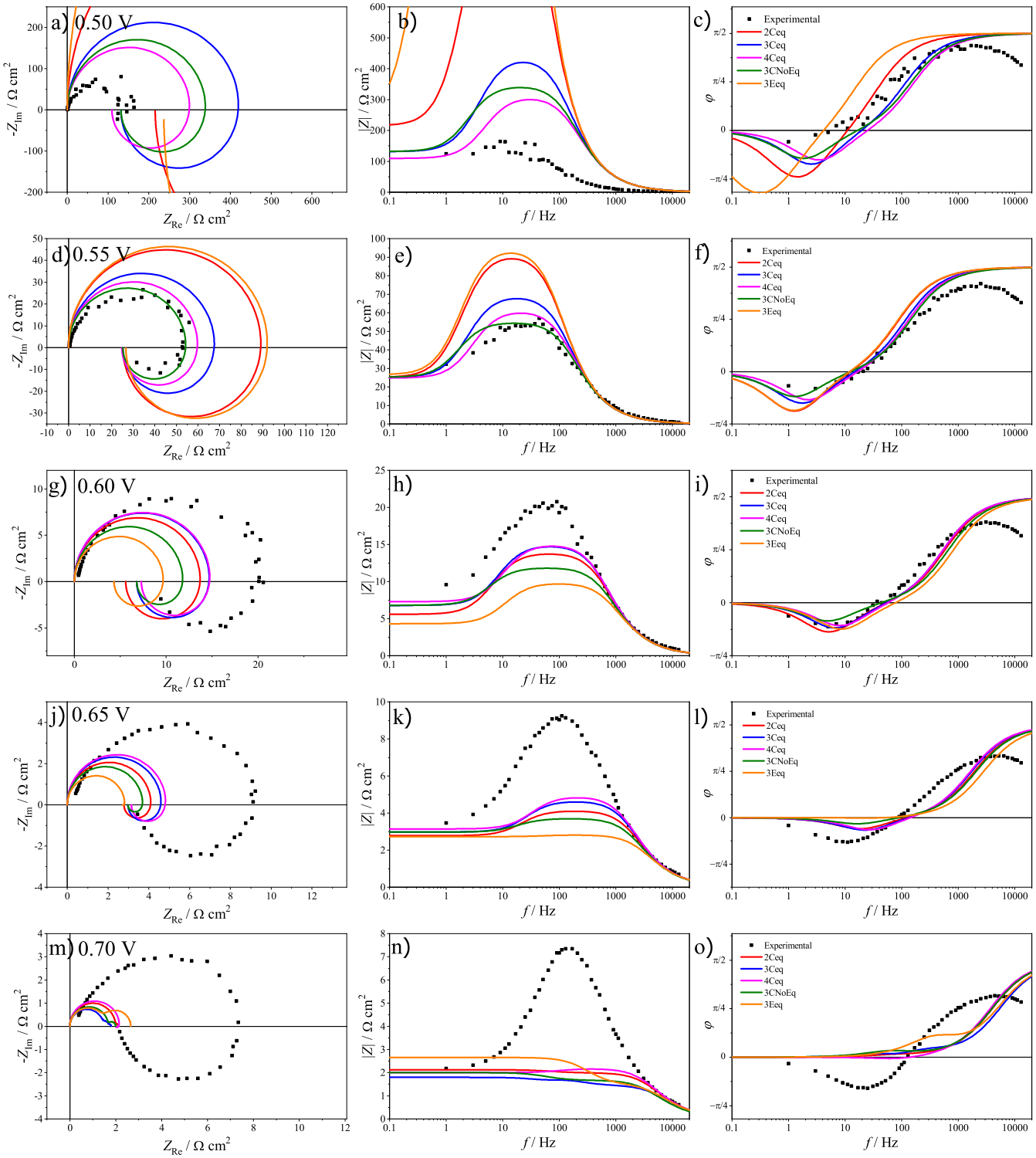

Figure 4: Experimental and modeled EIS spectra for selected potentials. Left, Nyquist plot, middle, magnitude vs frequency, and right, phase angle vs frequency. The potentials shown are a)-c) 0.50 V, d)-f) 0.55 V, g)-i) 0.60 V, j)-l) 0.65 V, and m)-o) 0.70 V. Showing the experimental value (black boxes), and the models 2Ceq (red), 3Ceq (blue), 4Ceq (purple), 3CNoEq (green), and 3Eeq (orange).

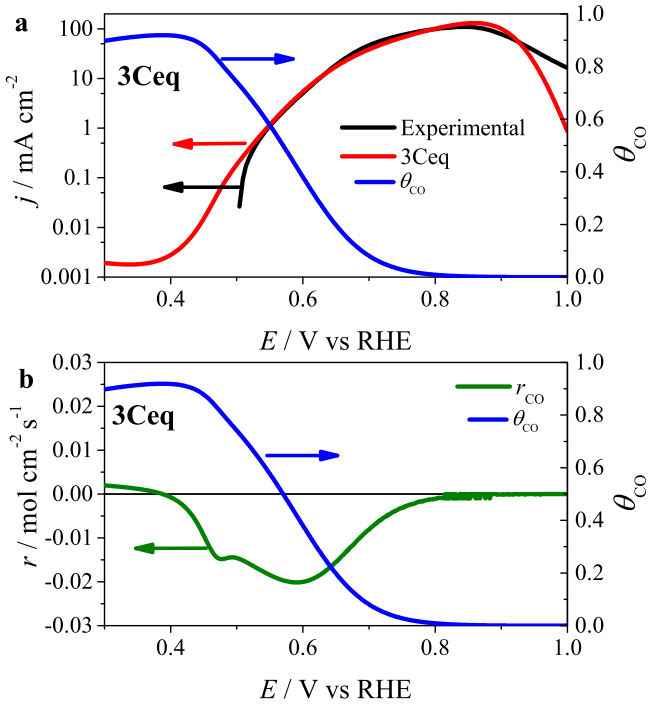

Figure 5: Comparison of the relative rates and the change in CO coverage, a) shows the total rate $= v_1 + 3v_{\mathrm{CO}} + v_{OH} + v_{CO_2} + v_{PtO}$ compared with the 3Ceq result and the CO coverage, θ_{CO}, b) shows the net CO rate, $r_{\mathrm{CO}} = v_1 - v_{\mathrm{COOH}}$, compared with the CO coverage, θ_{CO}.

high frequencies and an inductive loop at low frequecies, suggesting that the interplay between the production and removal rates of an adsorbate, here CO, is the source of the two features. Notably, this explains the trend in current vs potential reported in our previous work [13]. In that work, we argued that the overall response is controlled by both the methanol adsorption reaction and the surface reaction betweeen adsorbed intermediates, and that an increase in potential leads to net removal of CO. At that point, the shoulder peak corresponds with the flattening out of CO coverage, and the Tafel slope drops down to a value corresponding to methanol adsorption as the rate-determining step. For the rates seen in Fig. 5b, there is a minimum in CO removal rate at about 0.60 V, but no observable feature in the voltammograms. On the other hand, the shoulder peak, in this case at about 0.69 V, corresponds to where the CO coverage is low, here modeled to be 0.1. This will lead to a gradual transition to a rate limited fully by the methanol adsorption rate, and consequently decreases the apparent charge-transfer coefficient. At about 0.83 V, the main peak occurs where the CO coverage is practically zero and the OH coverage is rapidly increasing, see Fig. 3b. As commonly thought to be the case, this and subsequent surface oxidation eventually blocks the surface and decreases the rate of the MOR.

The method of analysis outlined in this work and previous works on this topic [13, 14] indicates that a better understanding of the reaction mechanism is possible through analysis of EIS data. A drawback of the approach used here is that the reaction mechanisms are still over-simplified. For example, the direct pathway is not included, adsorbate interaction is ignored, and the symmetry factors of individual reactions steps are assumed constant. However, these assumptions are common in the literature. While these assumptions may influence the conclusions reached in this work, the greatest drawback is that the reaction mechanisms is fitted to the data with the least amount of information, i.e., the cyclic voltammetry data. Therefore, an improvement of the method where the cyclic voltammetry and dEIS spectra are fitted simultaneously to optimize kinetic parameters is desirable. In particular, this would be an important step forward if one wants to include additonal parameters such as symmetry factors, Frumkin/Temkin factors during adsorption processes, and back reaction rate constants. A simultaneous fitting procedure is not computationally feasible without an improved algorithm, and this is currently being developed. Such a process would allow for an unprecedented detailed understanding of the reaction mechanism from a macroscopic point of view and would be a valuable support for studies approaching the problem at the micro level, i.e., first-principles calculations and studies using nanoparticles or single-crystals.

4. Conclusions

A mechanistic modeling study was done on cyclic voltammetry and dynamic electrochemical impedance spectroscopy (dEIS) data for methanol oxidation on Pt in 0.5 M H_2SO_4 at 100°C. In total, five different reaction models were proposed and tested and dEIS experimental results were used to distinguish between the models.

The analysis of the results supports the conclusions that i) water adsorption is reversible, and ii) the surface reaction between adsorbed CO and adsorbed OH is a chemical reaction.

The measurements confirmed previous observations for this reaction. For the indirect mechanism of methanol oxidaiton, water activation is the source of high overpotentials. After the onset of CO oxidation through the activation of water, the overall rate is determined by a combination of the dissociative methanol adsorption and the CO oxidation step until the shoulder peak. Beyond the shoulder peak, the overall rate is determined by the methanol adsorption step until the main peak.

The authors believe that the method demonstrated here can be optimized for other reactions and has potential widespread application.

Acknowledgment

This work was financially supported by the Natural Sciences and Engineering Research Council of Canada through

its Discovery Frontiers program (Engineered Nickel Catalysts for Electrochemical Clean Energy project administered from Queen's University, grant RGPNM 477963-2015) and Discovery Grants program (grant RGPIN-2017-04045), and by the Research Council of Norway through the FRIPRO (project 221899) and INTPART (project 261620) programs. T.H. thanks the Faculty of Natural Sciences at NTNU for a scholarship.

References

[1] D. D. Macdonald, Electrochimica Acta 35 (1990) 1509 – 1525.
[2] U. Krewer, M. Christov, T. Vidakovic, K. Sundmacher, Journal of Electroanalytical Chemistry 589 (2006) 148–159.
[3] G. Galicia, N. Pébère, B. Tribollet, V. Vivier, Corrosion Science 51 (2009) 1789 – 1794.
[4] D. S. Ramírez-Rico, E. R. Larios-Durán, Journal of The Electrochemical Society 164 (2017) H994–H1002.
[5] D. D. Macdonald, Electrochimica Acta 51 (2006) 1376–1388.
[6] A. Battistel, F. L. Mantia, Electrochimica Acta 304 (2019) 513–520.
[7] W. L. Underkofler, I. Shain, Analytical Chemistry 37 (1965) 218–222.
[8] A. M. Bond, R. J. O'Halloran, I. Ruzic, D. E. Smith, Journal of Electroanalytical Chemistry and Interfacial Electrochemistry 90 (1978) 381–388.
[9] D. A. Harrington, Journal of Electroanalytical Chemistry 355 (1993) 21–35.
[10] J. E. Garland, C. M. Pettit, D. Roy, Electrochimica Acta 49 (2004) 2623–2535.
[11] R. Sacci, D. Harrington, ECS Transactions 19 (2009) 31–42.
[12] R. Sacci, F. Seland, D. Harrington, Electrochimica Acta 131 (2014) 13–19.
[13] T. Holm, P. K. Dahlstrøm, S. Sunde, F. Seland, D. A. Harrington, Electrochimica Acta 295 (2019) 139–147.
[14] T. Holm, D. A. Harrington, ECS Transactions 85 (2018) 167–176.
[15] P. S. Kauranen, E. Skou, J. Munk, Journal of Electroanalytical Chemistry 404 (1996) 1–13.
[16] T. Holm, P. K. Dahlstrøm, S. Sunde, D. A. Harrington, F. Seland, ECS Transactions 75 (2016) 1055–1061.
[17] T. Holm, P. K. Dahlstrøm, O. S. Burheim, S. Sunde, D. A. Harrington, F. Seland, Electrochimica Acta 222 (2016) 1792–1799.
[18] G. S. Popkirov, R. N. Schindler, Review of Scientific Instruments 64 (1993) 3111–3115.
[19] D. A. Harrington, B. E. Conway, Electrochimica Acta 32 (1987) 1703–1712.
[20] D. A. Harrington, Journal of Electroanalytical Chemistry 449 (1998) 9–28.
[21] F. V. Olver, D. W. Lozier, R. F. Boisvert, C. W. Clark (Eds.), NIST Handbook of Mathematical Functions, NIST and Cambridge University Press, NY, Online at http://dlmf.nist.gov/3.4.E9, 2010, Sec 13.14.
[22] D. M. Bates, D. G. Watts, Nonlinear regresssion analysis and Its application, Wiley, 1988, p. 53.
[23] M. Chojak-Halseid, Z. Jusys, R. J. Behm, The Journal of Physical Chemistry C 114 (2010) 22573–22581.
[24] B. Beden, F. Hahn, S. Juanto, C. Lamy, J.-M. Leger, Journal of Electroanalytical Chemistry and Interfacial Electrochemistry 225 (1987) 215–225.
[25] S. Liu, L. Liao, Q. Tao, Y. Chen, S. Ye, Phys. Chem. Chem. Phys. 13 (2011) 9725–9735.
[26] H. A. Gasteiger, N. Marković, P. N. Ross, E. J. Cairns, Journal of The Electrochemical Society 141 (1994) 1795–1803.
[27] A. Cuesta, Journal of the American Chemical Society 128 (2006) 13332–13333.
[28] M. Neurock, M. Janik, A. Wieckowski, Faraday Discuss. 140 (2009) 363–378.
[29] Y. Chen, A. Miki, S. Ye, H. Sakai, M. Osawa, Journal of the American Chemical Society 125 (2003) 3680–3681.
[30] T. Yajima, H. Uchida, M. Watanabe, Journal of Physical Chemistry B 108 (2004) 2654.
[31] K. Kunimatsu, H. Hanawa, H. Uchida, M. Watanabe, Journal of Electroanalytical Chemistry 632 (2009) 1090–119.
[32] J. Rossmeisl, J. Nørskov, C. Taylor, M. Janik, M. Neurock, Journal of Physical Chemistry B 110 (2006) 21833–21839.
[33] J. Rossmeisl, P. Ferrin, G. A. Tritsaris, A. U. Nilekar, S. Koh, S. E. Bae, S. R. Brankovic, P. Strasser, M. Mavrikakis, Energy Environ. Sci. 5 (2012) 8335–8342.
[34] Y.-H. Fang, Z.-P. Liu, ACS Catalysis 4 (2014) 4364–4376.
[35] Y.-H. Fang, Z.-P. Liu, Surface Science 631 (2015) 42–47.
[36] Y. X. Chen, S. Ye, M. Heinen, Z. Jusys, M. Osawa, R. J. Behm, Journal of Physical Chemistry B 110 (2006) 9534–9544.
[37] N. M. Marković, H. A. Gasteiger, P. N. R. Jr, X. Jiang, I. Villegas, M. J. Weaver, Electrochimica Acta 40 (1995) 91–98.
[38] D. Kardash, J. Huang, C. Korzeniewski, Langmuir 16 (2000) 2019–2023.
[39] F. Seland, D. A. Harrington, R. Tunold, Electrochimica Acta 52 (2006) 773 – 779.
[40] D. A. Harrington, P. van den Driessche, Journal of Electroanalytical Chemistry 501 (2001) 222–234.
[41] T. Vidakovic, M. Christov, K. Sundmacher, Journal of Electroanalytical Chemistry 580 (2005) 105–121.